Mass-Transfer Enhancement by a Reversible Chemical Reaction Across the Interface of a Bubble Rising Under Stokes Flow

Franck Pigeonneau
Surface du Verre et Interfaces, UMR 125 CNRS/Saint-Gobain, 39 Quai Lucien Lefranc, BP 135, 93303 Aubervilliers Cedex, France

Marion Perrodin
Surface du Verre et Interfaces, UMR 125 CNRS/Saint-Gobain, 39 Quai Lucien Lefranc, BP 135, 93303 Aubervilliers Cedex, France

Institut de Mécanique des Fluides de Toulouse, Université de Toulouse, CNRS UMR 5502, 2 Allée du Professeur Camille Soula, 31400 Toulouse, France

Eric Climent
Institut de Mécanique des Fluides de Toulouse, Université de Toulouse, CNRS UMR 5502, 2 Allée du Professeur Camille Soula, 31400 Toulouse, France

DOI 10.1002/aic.14520
Published online June 18, 2014 in Wiley Online Library (wileyonlinelibrary.com)

Mass transfer around a bubble rising in a liquid under Stokes regime is investigated when a reversible chemical reaction, $A \rightleftharpoons B$, is taken into account. Four dimensionless parameters control the interfacial transfer rate: the Péclet and Damköhler numbers, the ratio of the diffusion coefficient of both species, and the reaction equilibrium constant. The mass-transfer equations are solved numerically with a finite element technique. A boundary layer approach is also proposed and solved with a coupled technique of finite difference and Chebyshev-spectral method. The equilibrium constant and the ratio of diffusion coefficients have a strong influence on the coupling between the chemical reaction and mass transfer leading to an increase of the Sherwood number. The interaction between the chemical reaction and advection is clearly established by the simulations. Conditions corresponding to Péclet number larger than the Damköhler number reduces the effect of the chemical reaction. © 2014 American Institute of Chemical Engineers *AIChE J*, 60: 3376–3388, 2014

Keywords: Sherwood number, chemical reaction, Stokes flow, boundary layer theory, bubble

Introduction

Many chemical engineering processes are based on the absorption or desorption of gaseous material into a liquid phase. During glass melting, bubbles are created due to chemical reactions between raw materials and undergo, further, mass transfer due to fining process enhancing the rate of bubbles removal.[1] Among many other industrial manufacturing processes, the treatment of molten steel by blowing gas in ladles[2] is concerned with mass transfer between dispersed bubbles and molten steel. For all processes, the performance of conversion depends on the mass-transfer coefficient between the dispersed and continuous phases and the interfacial specific area. This multiscale problem requires a comprehensive understanding of the transport phenomena between the two phases close to interfaces before investigating the industrial process at large scale.

Mass transfer in two-phase flows occurs often coupled with chemical reactions[3] in many industrial applications. The prediction of interfacial transfer coefficient due to simultaneous diffusion and chemical reaction is usually based on the assumption that the resistance to diffusion is localized in a thin film adjacent to the gas–liquid interface.[4,5] The thickness of this thin film is then related to the effect of the kinetics of chemical reactions. In such case, it is generally observed that the chemical reactions enhance mass transfer[6] when the reactant transfers through the interface. Higbie[7] and later Danckwerts[8] developed alternative models under the assumption of continual renewal of fluid at the interface. Olander[9] studied the effect on mass transfer of various first- and second-order reversible chemical reactions in one-dimensional problems. He compared carefully the two theories proposed in Refs. 7 and 8.

From the first contributions devoted to mass transfer with chemical reactions around a bubble or a drop moving in a

Current address of Marion Perrodin: Saint-Gobain Recherche, 39 Quai Lucien Lefranc, BP 135, 93303 Aubervilliers Cedex, France

Correspondence concerning this article should be addressed to F. Pigeonneau at franck.pigeonneau@saint-gobain.com.

© 2014 American Institute of Chemical Engineers

liquid, Ruckenstein et al.[10] determined the mass-transfer coefficient for a first-order irreversible reaction both for creeping and potential flows. Soung and Sears[11] investigated the effect of the irreversible chemical reactions in unsteady regime. Kleinman and Reed[12] determined the mass transfer for a quiescent spherical inclusion with a first-order irreversible reaction. They focused their investigation on the effect of reaction kinetics on the enhancement of mass transfer. These authors studied in Ref. 13 the situation of a moving drop, bubble or particle experiencing irreversible first-order chemical reaction. More recently, Juncu[14,15] determined the mass transfer around drop or bubble over a limited range of Péclet and Damköhler numbers for first- or second-order irreversible reactions. When the Reynolds number based on the relative bubble velocity is larger than 10, an accurate description of the two-phase flow is required. In the article,[16] Koynov et al. solved the two-phase flow problem with a front tracking interface method to follow the bubble/liquid interface coupled with mass transfer coupled to two irreversible reactions. The authors focused their work on the effect of bubble swarms and interaction between few bubbles. Wylock et al.[17] gave an important contribution in the field of mass transfer coupled with chemical reactions by determining the mass-transfer coefficients where four species and two reversible reactions are involved. They achieved a complementary work taking into account the interface contamination and the bubble shape in Ref. 18. Using volume of fluid method, Bothe et al.[19] determined the mass transfer for an irreversible chemical reaction of sulfite oxidation. The numerical simulations have been compared to experimental results using laser-induced fluorescence measurement technique. The determination of the mass-transfer coefficient for instantaneous reaction has been done by Pigeonneau[20] for a particular application devoted to the oxidation-reduction of iron in molten glass.

Despite these contributions, a large overview of the evolution of mass-transfer coefficients for large variation of Péclet and Damköhler numbers is still lacking. Numerical modeling of bubbly reactors needs closure laws for mass-transfer coefficient (corresponding in dimensionless for to Sherwood number as a function of the flow properties, i.e., Péclet, Damköhler, and Schmidt numbers). Moreover, it is admitted that chemical reactions yield a boundary layer whose thickness is scaled by the characteristic scale of the chemical kinetics. Advection leads also to the formation of boundary layer when the diffusion coefficient is sufficiently small. The interaction between these two boundary layers plays an important role on the determination of mass-transfer coefficient in chemical processes. It is inherent to all situations in which chemical reactions are involved. The main purpose of our work is to provide a comprehensive understanding of the interplay between diffusion, advection, and chemical reaction during mass transfer across the bubble interface. More precisely, we focus on the determination of the enhancement factor due to the chemical reaction on the rate of mass transfer.

For glass melting applications, the hydrodynamics is generally related to creeping flows, that is, small Reynolds number. Indeed, the smallest dynamic viscosity in glass furnace is around 10 Pa s, while the typical bubble size is smaller than 1 cm giving a Reynolds number much smaller than 1. The diffusion coefficients of gas species in molten glass are very small (around 10^{-10} m^2 s^{-1} at 1400°C) leading to a Schmidt number equal to 10^7, see for more details on the physical data in molten glass, the book of Scholze.[21] Consequently, the Péclet number, product of the Reynolds number by the Schmidt number is quite large ($\approx 10^6$) meaning that even if the flow motion in molten glass is in creeping regime, mass transfer is mainly driven by advection. In this article, the following issues are addressed: what is the effect of coupling phenomena such as advection, diffusion, and chemical reaction around a single rising bubble? What is the evolution of the enhancement factor when advection is more and more important? More specifically, we want to evaluate the interplay between those phenomena on the resulting boundary layer thickness (theoretical analysis leading to scaling laws). By varying the equilibrium constant different chemical regimes can be investigated where species are preferentially consumed or produced.

As it is impossible to embrace the study of mass transfer coupled with chemical reactions completely, this work is limited to the situation of one reversible chemical reaction between two species, that is, $A \rightleftarrows B$. The effect of the relative diffusion of both species is also addressed. The main purpose is to raise general results as a first step toward more complex situations.

To investigate the coupling between transport phenomena and chemical reaction over large range of Péclet and Damköhler numbers, two numerical approaches are used. Over a large range of Péclet number, a finite element technique is used to solve directly the general problem for low to moderate reaction kinetics. Nevertheless, when the chemical kinetics becomes very fast meaning that the Damköhler number is large or when the Péclet number is larger than 10^6, it is difficult to enforce accuracy on spatial resolution without a dramatic increase of computing time. Moreover, in these two limits, difficulties appear in term of numerical stability. To investigate properly the cases of large Damköhler and Péclet numbers, a coupled spectral-Chebyshev/finite difference method to solve the boundary layer formulation in the limit of high Péclet number has been developed for which the chemical kinetics is studied over a large range. It is then possible to obtain mass-transfer coefficients when the chemical reactions become instantaneous. We can compare the simulation results with asymptotic solutions validating the numerical method.

The article is organized as follows. First, the problem statement is presented in the second section in which the general and the boundary layer formulations are given followed by the numerical results and discussion. After the conclusion, two appendices are provided to detail the numerical methods and exact solutions for instantaneous chemical reaction.

Problem Statement

Transport equations for the species

We consider a spherical bubble, rising in a liquid at rest. Its radius, a, is assumed constant even in the presence of mass transfer. This assumption has been validated by Pigeonneau et al.[22] where it is shown that the time scale of the bubble radius variation is typically three orders of magnitude lower than the characteristic time of mass transfer. The interface between the bubble and the liquid is assumed completely mobile (shear free boundary condition). In the industrial context of glass melting, the last assumption has been verified experimentally by Jucha et al.,[23] Hornyak and Weinberg,[24] and Li and Scheider.[25] We assume the Reynolds

number to be small which corresponds to small bubbles rising in a viscous liquid (see Clift et al.[26] for practical conditions of spherical bubble and creeping flow to be matched simultaneously). Consequently, the general solution provided by Hadamard[27] or Rybczynski[28] is used to describe the flow motion around the bubble. The balance between the drag and the buoyancy forces gives the terminal velocity

$$V_t = \frac{ga^2}{3\nu}, \tag{1}$$

where g is the gravity acceleration, $\nu = \mu/\rho$ is the kinematic viscosity of the liquid and ρ the liquid density.

We consider two chemical species, A, the reactant, and B, the product, consumed and produced by a homogeneous reversible chemical reaction in the liquid

$$A \rightleftarrows B \tag{2}$$

with the equilibrium constant equal to

$$K_{eq} = \frac{C_{B_{eq}}}{C_{A_{eq}}} \tag{3}$$

The quantities C_A and C_B are the molar concentrations of the Solutes A and B in the liquid, respectively.

Due to symmetry, cylindrical polar coordinates, (r, φ, z), originating from the bubble center are used for which the φ-component of the velocity and all derivatives with respect to this coordinate are equal to zero. The general equations for the transport of C_A and C_B in the liquid experiencing advection, diffusion, and chemical reaction are

$$\frac{\partial C_A}{\partial t} + u_r \frac{\partial C_A}{\partial r} + u_z \frac{\partial C_A}{\partial z} = \mathcal{D}_A \times \left[\frac{1}{r}\frac{\partial}{\partial r}\left(r\frac{\partial C_A}{\partial r}\right) + \frac{\partial^2 C_A}{\partial z^2}\right] - k^+\left(C_A - \frac{C_B}{K_{eq}}\right) \tag{4}$$

$$\frac{\partial C_B}{\partial t} + u_r \frac{\partial C_B}{\partial r} + u_z \frac{\partial C_B}{\partial z} = \mathcal{D}_B \times \left[\frac{1}{r}\frac{\partial}{\partial r}\left(r\frac{\partial C_B}{\partial r}\right) + \frac{\partial^2 C_B}{\partial z^2}\right] + k^+\left(C_A - \frac{C_B}{K_{eq}}\right) \tag{5}$$

where t is the time, $\mathcal{D}_A$ and $\mathcal{D}_B$ are the diffusion coefficients of A and B, respectively. The quantity k^+ is the kinetic constant of reaction (2) toward production of B. The two velocity components of the steady flow, u_r and u_z, are determined according to Refs. 27 and 28 and will be given latter. Remark that the problem is written under unsteady formulation although we will analyze only steady state while transient effects have a negligible role on processes running 24 h a day.

To solve the coupled equations, boundary conditions are required. The bubble-liquid interface, Γ_b (see Figure A1), is assumed permeable to A and impermeable to B (zero flux boundary condition). In the bulk, at the infinity, the chemical equilibrium between A and B is achieved. To summarize, the boundary conditions are the following

$$C_A = C_A^S, \text{ on } \Gamma_b, C_A = C_A^\infty, \text{ when } ||\boldsymbol{x}|| \to \infty \tag{6}$$

$$\frac{\partial C_B}{\partial n} = 0, \text{ on } \Gamma_b, C_B = K_{eq} C_A^\infty, \text{ when } ||\boldsymbol{x}|| \to \infty \tag{7}$$

in which $\boldsymbol{x}$ represents the position of a point in the domain given by the coordinates (r, z) in the cylindrical polar coordinate system.

Dimensionless formulation

The numerical solution is achieved for a set of dimensionless equations. Only four dimensionless numbers are involved in the normalized mass balance equations. The characteristic length scale is the bubble diameter, $2a$. The velocity field is scaled by V_t. The dimensionless molar concentrations of A and B are written as follows

$$\bar{C}_A = \frac{C_A - C_A^\infty}{C_A^S - C_A^\infty}, \quad \bar{C}_B = \frac{C_B - K_{eq} C_A^\infty}{K_{eq}\left(C_A^S - C_A^\infty\right)} \tag{8}$$

Beside the equilibrium constant, already defined in Eq. (3), the three other dimensionless numbers are

$$Pe_A = \frac{2aV_t}{\mathcal{D}_A}, \ \mathrm{Da} = \frac{4a^2 k^+}{\mathcal{D}_A}, \ \bar{\mathcal{D}} = \frac{\mathcal{D}_B}{\mathcal{D}_A} \tag{9}$$

The first is the Péclet number based on the diffusion coefficient of A. The second dimensionless number is the Damköhler number written as the ratio of diffusion time of Species A to chemical reaction time of Eq. (2). Finally, the last dimensionless number is the ratio of the two diffusion coefficients.

Without the bar over the dimensionless variables, the dimensionless mass balance equations become

$$\frac{\partial C_A}{\partial t} + u_r \frac{\partial C_A}{\partial r} + u_z \frac{\partial C_A}{\partial z} = \frac{1}{Pe_A} \times \left[\frac{1}{r}\frac{\partial}{\partial r}\left(r\frac{\partial C_A}{\partial r}\right) + \frac{\partial^2 C_A}{\partial z^2}\right] - \frac{Da}{Pe_A}(C_A - C_B) \tag{10}$$

$$\frac{\partial C_B}{\partial t} + u_r \frac{\partial C_B}{\partial r} + u_z \frac{\partial C_B}{\partial z} = \frac{\mathcal{D}}{Pe_A} \times \left[\frac{1}{r}\frac{\partial}{\partial r}\left(r\frac{\partial C_B}{\partial r}\right) + \frac{\partial^2 C_B}{\partial z^2}\right] + \frac{Da}{K_{eq} Pe_A}(C_A - C_B) \tag{11}$$

The boundary conditions write

$$C_A = 1, \text{ on } \Gamma_b, C_A = 0, \text{ when } \boldsymbol{x} \to \infty \tag{12}$$

$$\frac{\partial C_B}{\partial n} = 0, \text{ on } \Gamma_b, C_B = 0, \text{ when } \boldsymbol{x} \to \infty \tag{13}$$

The dimensionless expressions for u_r and u_z, that is, velocity components divided by V_t, are

$$u_r = \frac{zr}{4\left(z^2 + r^2\right)^{3/2}}, \quad u_z = -1 + \frac{r^2 + 2z^2}{4\left(z^2 + r^2\right)^{3/2}} \tag{14}$$

When steady state is reached, the solution will be used to determine the Sherwood number over the bubble interface for Solute A by integration of the normal gradient of C_A over the bubble interface area as follows

$$Sh_A = -\frac{1}{\pi}\int_{\Gamma_b} \left.\frac{\partial C_A}{\partial n}\right|_{\Gamma_b} dS \tag{15}$$

This is a dimensionless measure of mass transfer averaged over the bubble surface (total mass transfer scaled by the pure diffusion solution).

Equations (10) and (11) with a velocity given by (14) and boundary conditions (12) and (13) have been solved by a Finite element technique for which all details have been reported in Appendix A.

Boundary layer approximation

When the Péclet number becomes large (typically larger than 10^3), concentrations C_A and C_B present strong gradients

close to the bubble interface. The Sherwood number scales with the square root of the Péclet number when Pe_A is larger than 10^3 for pure transfer.[29] In this section, a boundary layer approximation of the coupled equations is proposed to establish the asymptotic behaviour when the Péclet number is sufficiently large.

To write the boundary layer equations, spherical coordinates (R, θ, φ), with origin at the center of the bubble, are used. The radial coordinate, R, is equal to $\sqrt{r^2+z^2}$ and $\theta = \arctan(r/z)$, the polar angle. According to Hadamard–Rybczynski's solution, the radial u_R and polar u_θ velocity components are given in dimensionless form (divided by the terminal velocity) by

$$u_R = -\left(1-\frac{1}{2R}\right)\cos\theta, \quad u_\theta = \left(1-\frac{1}{4R}\right)\sin\theta \tag{16}$$

In spherical coordinates, conservation equations on C_A and C_B written under steady-state regime become

$$u_R\frac{\partial C_A}{\partial R} + \frac{u_\theta}{R}\frac{\partial C_A}{\partial \theta} = \frac{1}{R^2 Pe_A} \times\left[\frac{\partial}{\partial R}\left(R^2\frac{\partial C_A}{\partial R}\right) + \frac{1}{\sin\theta}\frac{\partial}{\partial\theta}\left(\sin\theta\frac{\partial C_A}{\partial\theta}\right)\right] - \frac{Da}{Pe_A}(C_A - C_B) \tag{17}$$

$$u_R\frac{\partial C_B}{\partial R} + \frac{u_\theta}{R}\frac{\partial C_B}{\partial \theta} = \frac{\mathcal{D}}{R^2 Pe_A} \times\left[\frac{\partial}{\partial R}\left(R^2\frac{\partial C_B}{\partial R}\right) + \frac{1}{\sin\theta}\frac{\partial}{\partial\theta}\left(\sin\theta\frac{\partial C_B}{\partial\theta}\right)\right] + \frac{Da}{K_{eq}Pe_A}(C_A - C_B) \tag{18}$$

To find the boundary layer equations, the radial coordinate is written as follows

$$R = \frac{1+\delta\zeta}{2} \tag{19}$$

where δ is a constant proportional to the boundary layer thickness and ζ is the inner coordinate.[30] Using (19), Eqs. (17) and (18) become

$$\frac{u_R}{\delta}\frac{\partial C_A}{\partial\zeta} + \frac{u_\theta}{1+\delta\zeta}\frac{\partial C_A}{\partial\theta} = \frac{2}{\delta^2 Pe_A(1+\delta\zeta)^2} \times\left\{\frac{\partial}{\partial\zeta}\left[(1+\delta\zeta)^2\frac{\partial C_A}{\partial\zeta}\right] + \frac{1}{\sin\theta}\frac{\partial}{\partial\theta}\left(\sin\theta\frac{\partial C_A}{\partial\theta}\right)\right\} - \frac{Da}{2Pe_A}(C_A - C_B) \tag{20}$$

$$\frac{u_R}{\delta}\frac{\partial C_B}{\partial\zeta} + \frac{u_\theta}{1+\delta\zeta}\frac{\partial C_B}{\partial\theta} = \frac{2\mathcal{D}}{\delta^2 Pe_A(1+\delta\zeta)^2} \times\left\{\frac{\partial}{\partial\zeta}\left[(1+\delta\zeta)^2\frac{\partial C_B}{\partial\zeta}\right) + \frac{1}{\sin\theta}\frac{\partial}{\partial\theta}\left(\sin\theta\frac{\partial C_B}{\partial\theta}\right)\right\} + \frac{Da}{2K_{eq}Pe_A}(C_A - C_B) \tag{21}$$

The velocity components, u_R and u_θ have been expanded as a function of δ.[20,31] In this approach Pe_A is no longer an independent parameter as it is assumed large, we write the Damköhler number proportional to the Péclet number, that is

$$Da = 2\alpha Pe_A \tag{22}$$

In the last relation, α is a new dimensionless number which can be written using the definition of Da and Pe_A given by (9) by

$$\alpha = \frac{ak^+}{V_t} \tag{23}$$

Consequently, α is the product of the kinetic constant of the reaction by the time scale of advection meaning that this quantity will be large when the chemical kinetics is very fast. To keep the reaction source terms in the boundary layer formulation, we assume that α is of order one.

According to the principle of least degeneracy of boundary conditions,[30,32] δ has to be equal to

$$\delta = \sqrt{\frac{2}{Pe_A}} \tag{24}$$

Therefore, the final expressions of the boundary layer equations at the zeroth order using the new variable

$$\mu = -\cos\theta \tag{25}$$

are

$$\zeta\mu\frac{\partial C_A}{\partial\zeta} + \frac{1-\mu^2}{2}\frac{\partial C_A}{\partial\mu} = \frac{\partial^2 C_A}{\partial\zeta^2} - \alpha(C_A - C_B) \tag{26}$$

$$\zeta\mu\frac{\partial C_B}{\partial\zeta} + \frac{1-\mu^2}{2}\frac{\partial C_B}{\partial\mu} = \mathcal{D}\frac{\partial^2 C_B}{\partial\zeta^2} + \frac{\alpha}{K_{eq}}(C_A - C_B) \tag{27}$$

with the boundary conditions

$$C_A = 1, \text{ for } \zeta = 0, \lim_{\zeta\to\infty} C_A = 0 \tag{28}$$

$$\frac{\partial C_B}{\partial\zeta} = 0, \text{ for } \zeta = 0, \lim_{\zeta\to\infty} C_B = 0 \tag{29}$$

The Sherwood number in the boundary layer formulation is given by the following relation

$$Sh_A = -\sqrt{\frac{Pe_A}{2}}\int_{-1}^{1}\left.\frac{\partial C_A}{\partial\zeta}\right|_{\zeta=0} d\mu \tag{30}$$

With the reversible reaction, we did not find any self-similar solution of the system of Eqs. (26) and (27). Consequently, a numerical method will be used to solve the boundary layer equations. The details about the numerical method are presented in Appendix A.

Results and Discussion

Numerical results are presented successively with the two methods used in this work starting with the boundary layer formulation and then with the finite element method for direct numerical simulations. To verify the numerical accuracy, asymptotic solutions will be established and also used to understand the physics of the problem.

Boundary layer approximation

In this section, the results provided by the boundary layer equations (see Section Boundary layer approximation under Problem Statement) are presented. When the chemical reaction consumes the gas transferring from the bubble, the mass transfer is expected to increase. The enhancement factor is defined by

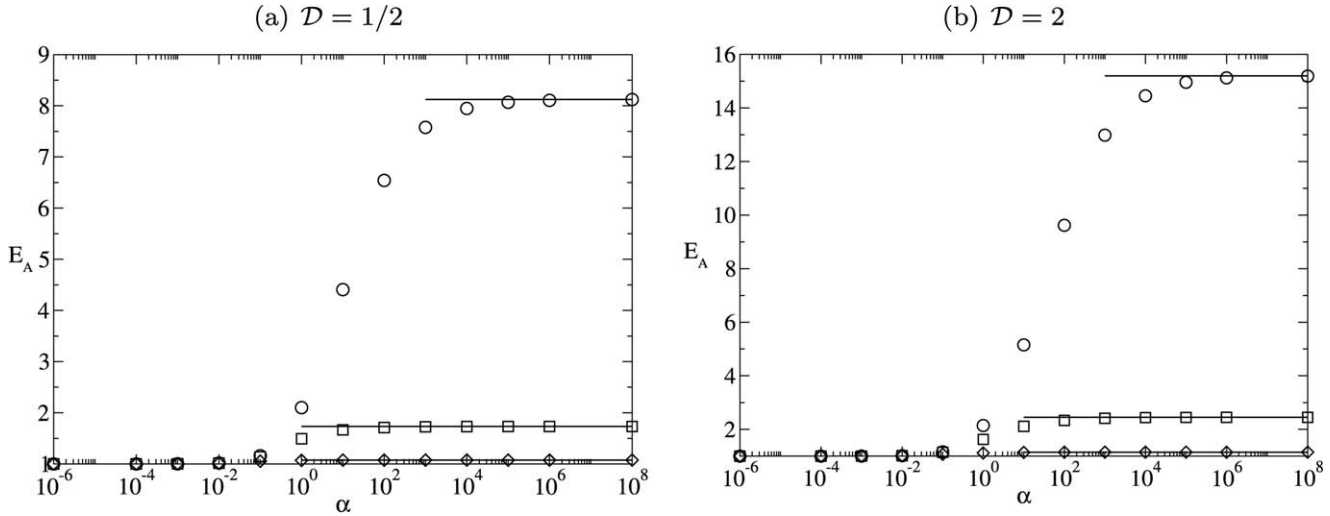

Figure 1. E_A as a function of α for (a) $\mathcal{D} = 1/2$ and (b) $\mathcal{D} = 2$ and for $K_{eq} = 10$ (○), $K_{eq} = 1$ (□), and $K_{eq} = 10^{-1}$ (◇).

Solid lines correspond to the asymptotic solution given by Eq. (33) for large α.

$$E_A = \frac{Sh_A(Pe_A, \alpha)}{Sh_A(Pe_A, \alpha=0)} \tag{31}$$

where $Sh_A(Pe_A, \alpha=0)$ corresponds to the Sherwood number without chemical reaction obtained in the boundary layer regime by[29]

$$Sh_A(Pe_A, \alpha=0) = \frac{2}{\sqrt{3\pi}}\sqrt{Pe_A} \approx 0.651\sqrt{Pe_A} \tag{32}$$

The boundary layer formulation depends on three dimensionless parameters: α, $\mathcal{D}$, and K_{eq} while Pe_A is assumed to be large. To study the influence of the reaction kinetics, we performed numerical simulations over a large range of α. Figure 1 presents the enhancement factor as a function of α for two values of $\mathcal{D}$ equal to 1/2 and 2. Three values of the equilibrium constant are tested: 10, 1, and 0.1. As expected, when α is very small the enhancement factor tends to one meaning that the chemical reaction does not play any role on mass transfer. When α becomes larger than one, E_A increases significantly to reach an asymptotic value at very high α. The results show that the equilibrium constant influences both the magnitude of the enhancement factor and the range of α over which E_A is well approximated by the asymptotic regime at large α. The asymptotic behavior is reached for smaller value of α when the equilibrium constant is small.

Mass transfer of Species A is, therefore, enhanced when the equilibrium constant is larger than one corresponding to consumption of A and production of B. An increase of the diffusion coefficient of Species B is also an important factor to promote the role of the chemical reaction.

To determine the enhancement factor when the chemical reaction becomes instantaneous, that is, infinite value of α, an exact solution of the boundary layer equations according to Olander[9] has been provided in Appendix B. It is shown that the two transport equations of A and B concentrations can be reduced to only one equation without chemical source term for the quantity equal to $C_A + K_{eq} C_B$. The solution is obtained by decomposing the domain outside the bubble in two regions: the former corresponds to the inner region close to the bubble interface where the chemical reaction does not reach equilibrium and the latter where the chemical equilibrium is reached meaning that $C_A = C_B$. Using simultaneously that in the inner region the gradient of $C_A + K_{eq}\mathcal{D}C_B$ is constant (see details in Appendix B) and that the gradient of C_B is equal to zero at the bubble interface, the interfacial mass flux of A is directly given by Eq. (B5). This provides an analytic prediction of the enhancement factor assuming chemical equilibrium

$$E_A(Pe_A, \alpha \to \infty) = \sqrt{(1+K_{eq})(1+\mathcal{D}K_{eq})} \tag{33}$$

This is exactly the same relation established by Olander[9] in the Cartesian geometry for unsteady transfer. This corresponds to the surface-renewal mechanism which is actually the situation experienced by a bubble rising in a liquid. Remark that Crank[33] proposed a model to describe diffusion process coupled with an instantaneous irreversible reaction for immobilized reactant A. Here, we extend this model for a nondiffusive product, Species B. Indeed, if $\mathcal{D}$ tends to zero in Eq. (33), the enhancement factor is simply equal to $\sqrt{1+K_{eq}}$. Similar approach has been followed to describe the mass transfer of oxygen in molten glass in Refs. 20 and [34] where the enhancement factors are quite similar to our results.

To verify those theoretical predictions, the solution of boundary layer equations has been obtained to determine the enhancement factor assuming chemical equilibrium. Figure 2 shows E_A vs. K_{eq} for $\alpha = 10^8$ and for four diffusion ratios. When the chemical reaction is in favor of production of B (large value of K_{eq}) mass transfer is significantly enhanced. For a diffusion ratio equal to 10^{-4}, the enhancement factor is approximately equal to 10 when $K_{eq} = 10^2$ which agrees with $\sqrt{1+K_{eq}}$. Moreover, the chemical reaction is more and more efficient when $\mathcal{D} > 1$ (higher diffusion of B than A).

The solid line in Figure 2 represents the solution (33) which is in perfect agreement with the numerical results obtained from the boundary layer formulation. When $K_{eq} \gg 1$, two scaling laws can be derived for the enhancement factor $E_A \sim \sqrt{\mathcal{D}K_{eq}}$ for $\mathcal{D} \gg 1$ and $E_A \sim \sqrt{K_{eq}}$ for $\mathcal{D} \ll 1$ (see Figure 2 where the two asymptotic behaviors have been plotted with dashed lines when K_{eq} is larger than 10).

Numerical solutions for arbitrary Pe_A

The mass transfer involving a reversible chemical reaction between two species is investigated over a large range of Péclet number by direct simulations of transport equations.

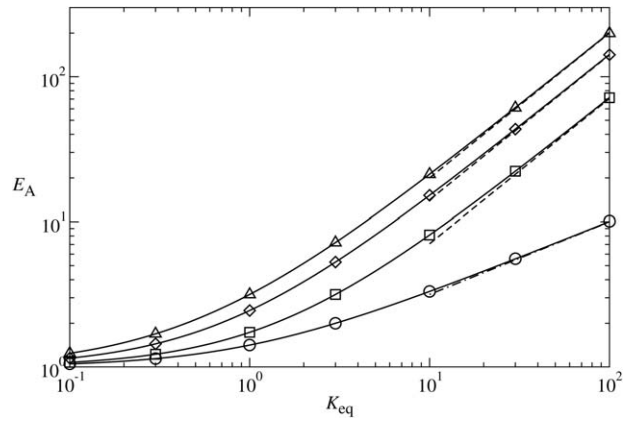

Figure 2. E_A as a function of K_{eq} obtained with $\alpha = 10^8$ when $\mathcal{D} = 10^{-4}$ (○) $\mathcal{D} = 1/2$ (□) $\mathcal{D} = 2$ (◇), and $\mathcal{D} = 4$ (△).

The solid line is the solution given by Eq. (33).

The numerical results have been obtained for Péclet number ranging from 10^{-3} to 10^6. As in the previous subsection, the equilibrium constant is equal to 10, 1, or 10^{-1}.

Figure 3 shows the evolution of the Sherwood number for Species A computed with relation (15) as a function of Pe_A when $\mathcal{D}=1/2$, and (a) $K_{eq}=10$, (b) $K_{eq}=1$, and (c) $K_{eq}=10^{-1}$. Seven values of Da have been investigated ranging from 1 to 10^6. Results with the chemical reaction are compared to the correlation given by Clift et al.[26] without reaction (Figure 3).

As expected, the chemical reaction enhances the mass transfer for any value of the Péclet number. At a fixed value of the Péclet number, the Sherwood number increases with the Damköhler number to reach an asymptotic value at very large Da. For a fixed Damköhler number, we observe an unexpected behavior. Indeed, when the Péclet number increases, the effect of chemical reaction on mass transfer becomes less important. As shown in Figure 3a, the Sherwood number obtained in the presence of chemical reaction becomes closer to the solution without reaction when the Péclet number increases.

As observed in the previous results obtained from the boundary layer approximation, the enhancement due to chemical reaction depends strongly on the equilibrium constant. When $K_{eq}=10$, the increase of the Sherwood number is significant (Figure 3a). The enhancement remains

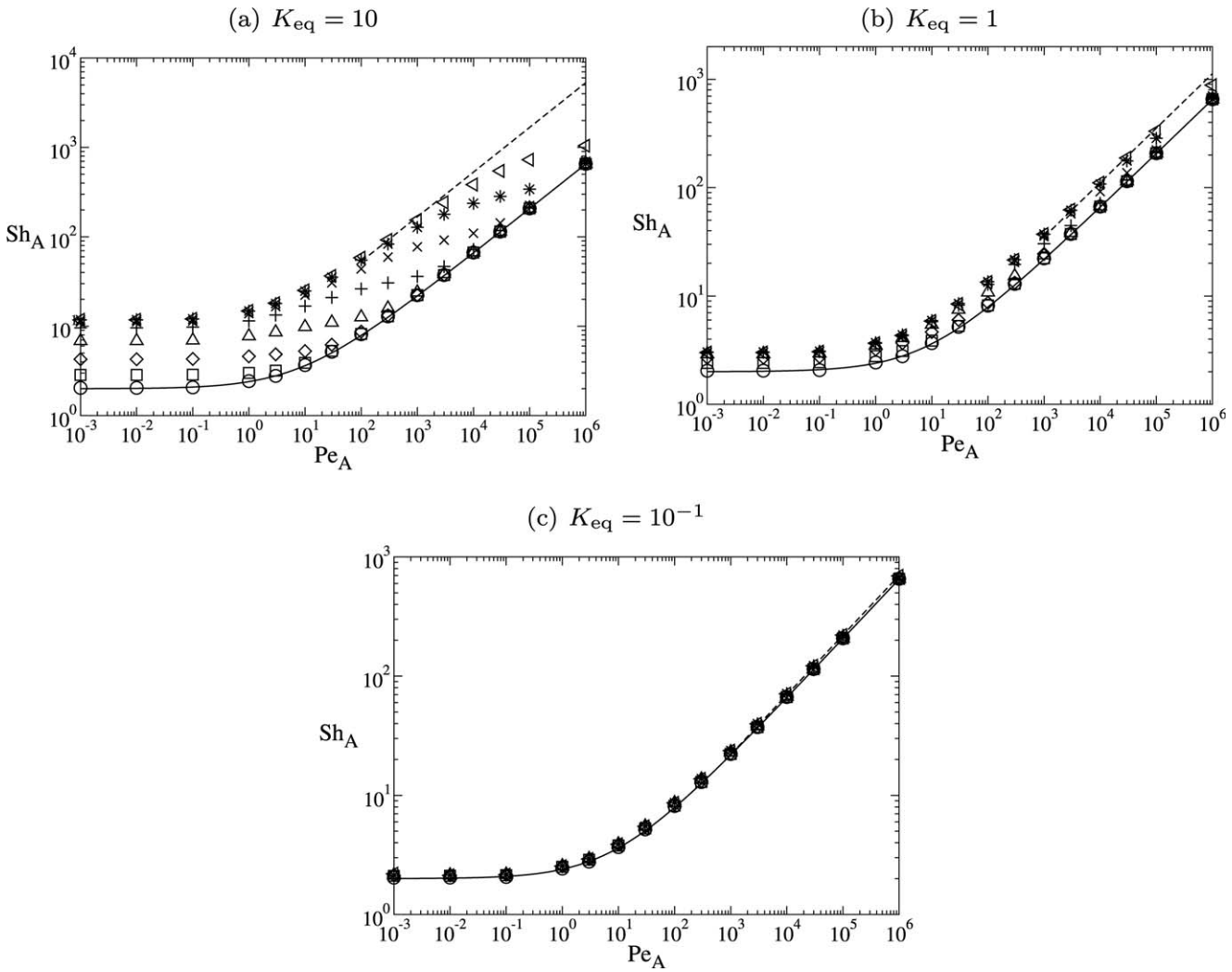

Figure 3. Sh_A as a function of Pe_A for $\mathcal{D} = 1/2$, for $Da = 0$ (○), 1 (□), 10 (◇), 10^2 (Δ), 10^3 (+), 10^4 (×), 10^5 (*), and 10^6 (◁) and for (a) $K_{eq} = 10$, (b) $K_{eq} = 1$, and (c) $K_{eq} = 10^{-1}$.

The solid line is the correlation given by Clift et al.[26] The dashed line is the curve obtaining from the boundary layer solution for an instantaneous reaction following the asymptotic behavior, Eq. (33).

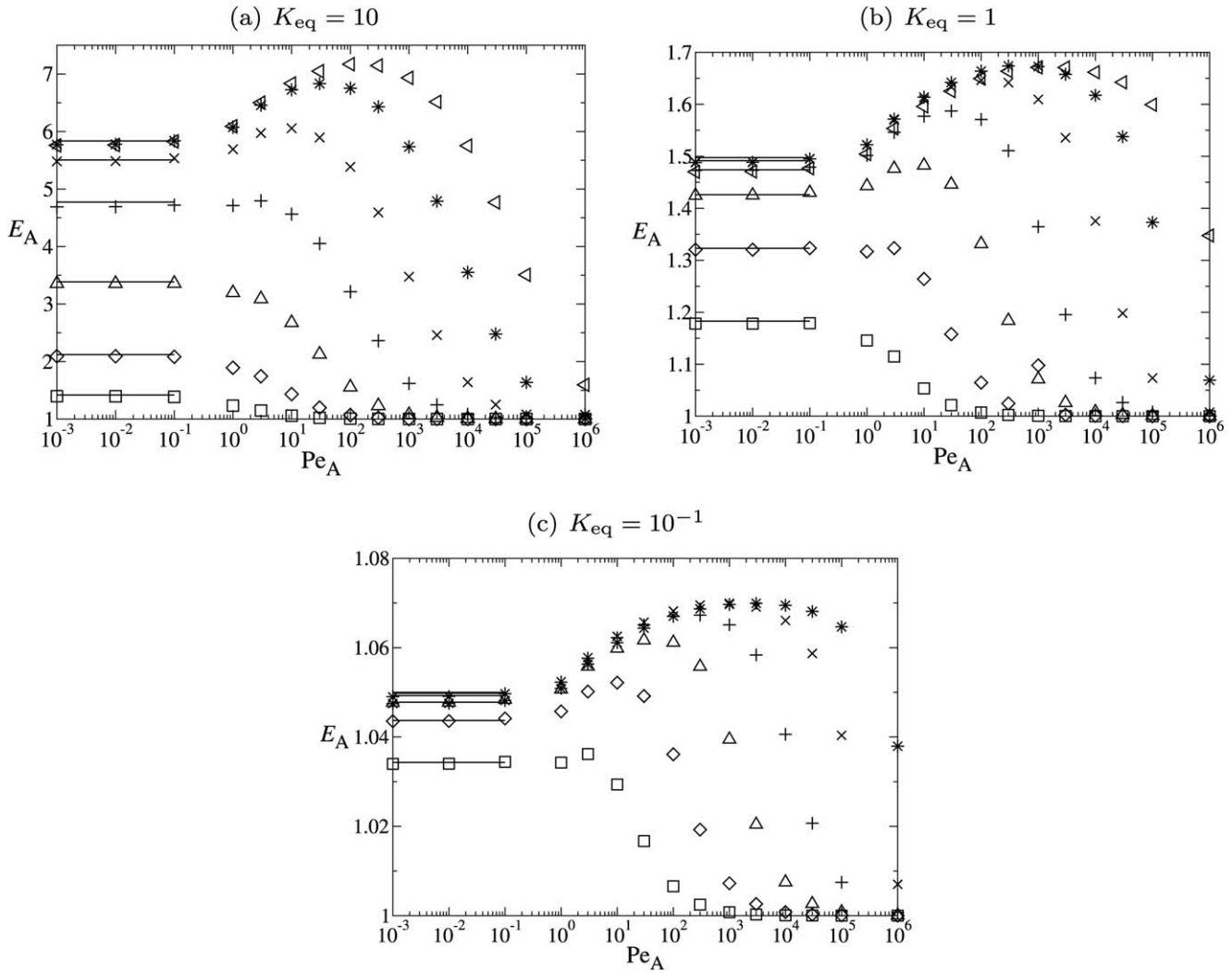

Figure 4. E_A as a function of Pe_A for $\mathcal{D} = 1/2$, for $Da = 1$ (□), 10 (◇), 10^2 (Δ), 10^3 (+), 10^4 (×), 10^5 (*), and 10^6 (◁) and for (a) $K_{eq} = 10$, (b) $K_{eq} = 1$, and (c) $K_{eq} = 10^{-1}$.

moderate for $K_{eq} = 1$ and finally vanishes for $K_{eq} = 10^{-1}$ (Figure 3c). When the kinetics of the chemical reaction becomes very important (large value of Damköhler number), the Sherwood number is expected to reach an asymptotic value. From the previous results provided by the boundary layer solution, the behavior of the Sherwood number for an instantaneous reaction can be determined. The dashed lines in Figure 3 represent the solution given by Eq. (33). Results obtained from the finite element method for the largest Damköhler number tend to the asymptotic behavior when the Péclet number is sufficiently large to stand in the boundary layer regime.

To highlight the respective importance of the advection and chemical reaction, the enhancement factor is determined as the ratio of the Sherwood number at a specific value of Da to the Sherwood number obtained without chemical reaction. This is similar to the one given by Eq. (31) for which the Sherwood number becomes a function of Pe_A, and Da. Figure 4 presents E_A as a function of Pe_A when $\mathcal{D} = 1/2$ and for seven values of the Damköhler number and with (a) $K_{eq} = 10$, (b) $K_{eq} = 1$, and (c) $K_{eq} = 10^{-1}$. For the equilibrium constant $K_{eq} = 10$, the enhancement factor reaches a value close to 7 while the maximum of E_A is only equal to 1.7 when $K_{eq} = 1$. For the smallest equilibrium constant, $K_{eq} = 10^{-1}$, the enhancement factor is no larger than 1.07 meaning that mass-transfer rate increases only a few percent in presence of chemical reaction. Note that whatever the value of equilibrium constant, E_A behaves nonmonotonically as a function of the Péclet number. A particular optimum of the reaction-induced enhancement is observed for each Damköhler number.

For low Péclet numbers, the enhancement factor becomes constant corresponding to the diffusive regime. Moreover, E_A increases with the Damköhler number to reach an asymptotic value at very high Da. To predict the evolution of the enhancement factor when advective terms vanish, an exact solution of the transport equations of A and B is derived in Appendix B (solution of the Laplacian operator in spherical polar coordinates). Thanks to the exact solution (B15), the Sherwood number can be estimated as follows

$$\lim_{Pe \to 0} Sh_A = 2\left(1 + K_{eq}\mathcal{D}\right) \frac{1 + 2\sqrt{\frac{K_{eq}\mathcal{D}}{\left(1+K_{eq}\mathcal{D}\right)Da}}}{1 + 2\sqrt{\frac{\left(1+K_{eq}\mathcal{D}\right)K_{eq}\mathcal{D}}{Da}}} \tag{34}$$

For a fast chemical reaction corresponding to very large Da, the Sherwood number reaches the following limit

$$\lim_{Pe\to 0,\, Da\to\infty} Sh_A = 2\left(1+K_{eq}\mathcal{D}\right) \tag{35}$$

which shows that the mass-transfer coefficient increases with the equilibrium constant and the ratio of diffusion coefficients $\mathcal{D}$. Remark that the enhancement factor E_A is equal to Sh_A given by (34) and (35) divided by two (which corresponds to pure diffusion) when the Péclet number tends to zero. It is noteworthy that when the diffusion coefficient of B tends to zero, the enhancement factor becomes equal to one even in the limit of high Damköhler number in the diffusive regime. This behavior is not observed for large Péclet number for which the enhancement factor is always larger than one when $\mathcal{D}$ tends to zero. This is due to the strong reduction of the convective terms in the limit of small Péclet number.

At large Péclet number, the evolution of the Sherwood number becomes close to the solution without chemical reaction. The precise value of Pe_A for which it happens depends on both the Damköhler and Péclet numbers due to the competition between the advection and chemical reaction. Figure 4 shows that E_A reaches a value close to one for a Péclet number depending on Da and $K_{eq.}$ The larger the Damköhler number, the larger has to be the Péclet number to match this particular regime. Moreover, the value of Pe_A for which E_A is close to one decreases with the equilibrium constant.

The reduction of the chemical reaction effect when the Péclet number increases can be explained by the interaction between the two boundary layers (due to the advection or the chemical reaction). From Eqs. (20) and (21), two boundary layer thicknesses can be estimated. The first corresponds to the boundary layer for the Species A and the second for the Species B. The typical thicknesses of the boundary layers are

$$\delta_A = \min\left(\frac{1}{\sqrt{Pe_A}}, \frac{1}{\sqrt{Da}}\right) \tag{36}$$

$$\delta_B = \min\left(\sqrt{\frac{\mathcal{D}}{Pe_A}}, \sqrt{\frac{\mathcal{D}K_{eq}}{Da}}\right) \tag{37}$$

From Eq. (37), advection becomes dominant when the Péclet number exceeds the ratio Da/K_{eq}. This criterion is very well verified in Figure 4 where we can see that for a Damköhler number equal to 10^3, advection controls mass transfer when Pe_A is approximately equal to 10^4 for an equilibrium constant, $K_{eq}=10$, whereas the Péclet number must be equal to 10^6 for $K_{eq}=10^{-1}$ which is two orders of magnitude larger. Such results show that the competition between advection and chemical reaction is driven by the boundary layer observed on Species B and this is not depending on the diffusion ratio $\mathcal{D}$.

The results obtained from the two methods proposed in this article can be compared more evidently. In the previous section devoted to the boundary layer analysis, the effect of the reaction kinetics has been studied thanks to the parameter α. Because this last quantity is proportional to the ratio of Da to Pe_A, those results can be determined in the diagram Sh_A vs. Pe_A. In Figure 5, this has been done for $K_{eq}=10$ and for two diffusion ratios $\mathcal{D}$ equal to 1/2 and 2. The results for two Damköhler numbers 10^5 and 10^6 have been presented.

The behavior of the Sherwood number obtained for a given Damköhler number when the Péclet number increases is in agreement for the two numerical methods. Indeed, as

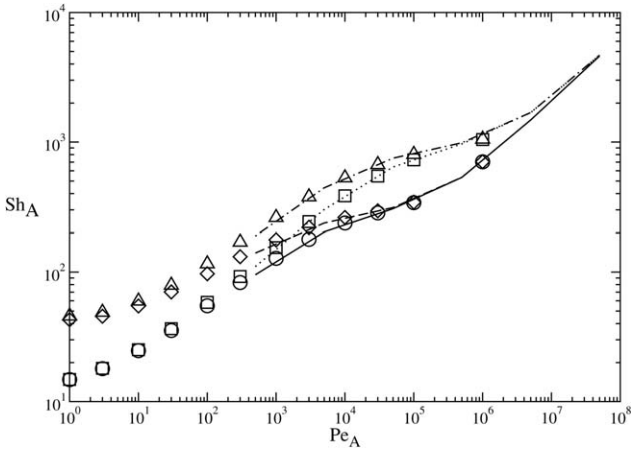

Figure 5. Sh_A as a function of Pe_A obtained from the finite element method for $K_{eq}=10$ and for $\mathcal{D}=1/2$ and $Da=10^5$ (○), $\mathcal{D}=1/2$ and $Da=10^6$ (□), $\mathcal{D}=2$ and $Da=10^5$ (◇), $\mathcal{D}=2$ and $Da=10^6$ (Δ).

The boundary layer solution is plotted for $\mathcal{D}=1/2$ and $Da=10^5$ (solid line), $\mathcal{D}=1/2$ and $Da=10^6$ (dotted line), $\mathcal{D}=2$ and $Da=10^5$ (dashed line) and $\mathcal{D}=2$ and $Da=10^6$ (dotted-dashed line).

the mass transfer is expected to increase with the Damköhler number, the Sherwood number obtained at $Da=10^6$ must be larger than one obtained at $Da=10^5$ which is verified in Figure 5. Furthermore, the threshold for which the advection dominates the chemical process is effectively observed for the same value of the Péclet number whatever the diffusion ratio. This conclusion can be drawn from Figure 5 where the curves obtained for two values of diffusion ratio merge at the same Péclet number. Consequently, the competition between advection and the reaction kinetics is indeed driven by the boundary layer of Species B.

Conclusions

Mass transfer around a spherical bubble rising in a viscous fluid has been studied when a homogeneous reversible chemical reaction between two species takes place in the liquid. The hydrodynamics is assumed to be in the Stokes regime corresponding to low Reynolds number based on the slip velocity and the bubble size. We addressed in particular the effect of the chemical reaction on the mass-transfer coefficient for a permeable reactant. The product is assumed impermeable at the bubble interface. The problem is written under dimensionless form leading to four parameters controlling the transfer. The first two parameters are related to the chemical reaction: the equilibrium constant controlling the direction of the chemical reaction and the Damköhler number measuring the importance of the chemical kinetics compared to diffusion. The two last are related to the physical process: the diffusion coefficient ratio comparing the relative importance of product and reactant diffusion and the Péclet number which is the ratio of the characteristic time of advection to the characteristic time of diffusion. The two mass balance equations are solved using two methods: direct numerical simulation based on a finite element method leading to results over a large range of Péclet number and boundary layer approximation to emphasize the coupling between the chemical kinetics and the advection process when the Péclet number is sufficiently large.

In general, an enhancement of the mass transfer is expected when a chemical reaction is involved. This is exactly what we found but it is noteworthy that the enhancement can be limited due to the importance of the advection process. Indeed, the chemical reaction leads to the development of a boundary layer which depends on the kinetic constant. Consequently, the mass transfer is enhanced due to the formation of this boundary layer. Nevertheless, when advection becomes more important (large value of the Péclet number) the boundary layer created by the flow transport contributes to mass transfer, as well. If the typical size of this advective boundary layer, scaling as the square root of the Péclet number, becomes smaller than the one due to the chemical reaction, the effect of the chemical reaction vanishes.

We pointed out the influence of the equilibrium constant which favors the production or consumption of species. When the equilibrium constant is larger than one meaning that the reaction is directed toward the production of B, the chemical reaction plays an important role on the interfacial mass transfer of A: the rate of mass transfer can be multiplied by a factor larger than 10. The enhancement of the mass-transfer coefficient is also more important when the diffusion coefficient of the product is larger than the diffusion coefficient of the reactant. Inversely, when the equilibrium constant is smaller than one, the chemical reaction does not play a significant role on mass transfer (the results we obtained are close to the situation of pure transfer without chemical reaction).

Finally, we showed that the Péclet number for which the advection process dominates does not depend on the diffusion ratio but is related to the equilibrium constant. This means that the competition between the chemical process and the advection is controlled by the physical transport of the product.

Apart from the numerical investigation, approximated solutions have been also established in this work in the limit of no advection and in the boundary layer when the chemical reaction becomes instantaneous. The enhancement due to chemical reaction can be easily estimated from these simplified relations. These results justify the model developed in Refs. 20 and 34 to describe the important role of the oxidation-reduction reaction of iron in molten glass.

This work has been done in Stokes regime. Nevertheless, many applications in chemical engineering are facing nonzero Reynolds numbers and nonspherical bubbles. So, this work has to be extended to other hydrodynamic regimes. Moreover, different reaction models and simultaneous multiple reactions must be investigated.

Literature Cited

1. Shelby JE. *Introduction to Glass Science and Technology*. Cambridge: The Royal Society of Chemistry, 1997.
2. Mazumdar D, Guthrie RIL. The physical and mathematical modelling of gas stirred ladle systems. *ISIJ Int*. 1995;35(1):1–20.
3. Sherwood TK, Wei JC. Interfacial phenomena in liquid extraction. *Ind Eng Chem.* 1957;49(6):1030–1034.
4. Lewis WK, Whitman WG. Principles of gas absorption. *Ind Eng Chem*. 1924;16(12):1215–1220.
5. Sherwood TK, Pigford RL. Absorption and Extraction. New York: McGraw-Hill Book Company, Inc., 1952.
6. Levenspiel O. Chemical Reaction Engineering. New York: Wiley, 1972.
7. Higbie R. The rate of absorption of a pure gas into a still liquid during short periods of exposure. *Tran Am Inst Chem Eng*. 1935;31: 365–389.
8. Danckwerts PV. Significance of liquid-film coefficients in gas absorption. *Ind Eng Chem*. 1951;43(6):1460–1467.
9. Olander DR. Simultaneous mass transfer and equilibrium chemical reaction. *AIChE J*. 1960;6(2):233–239.
10. Ruckenstein E, Dang VD, Gill WN. Mass transfer with chemical reaction from spherical one or two components bubbles or drops. *Chem Eng Sci*. 1971;26:647–668.
11. Soung WY, Sears JT. Effects of reaction order and convection around gas-bubbles in a gas-liquid reacting system. *Chem Eng Sci*. 1975;30(6):1353–1356.
12. Kleinman LS, Reed XBJ. Interphase mass transfer from bubbles, drops, and solid spheres: diffusional transport enhanced by external chemical reaction. *Ind Eng Chem Res*. 1995;34:3621–3631.
13. Kleinman LS, Reed XBJ. Unsteady conjugate mass transfer between a single droplet and an ambient flow with external chemical reaction. *Ind Eng Chem Res*. 1996;35(9):2875–2888.
14. Juncu G. Unsteady heat and/or mass transfer from a fluid sphere in creeping flow. *Int J Heat Mass Transfer*. 2001;44:2239–2246.
15. Juncu G. The influence of the Henry number on the conjugate mass transfer from a sphere: II - mass transfer accompanied by a first-order chemical reaction. *Heat Mass Transfer*. 2002;38:523–534.
16. Koynov A, Khinast JG, Tryggvason G. Mass transfer and chemical reactions in bubble swarms with dynamic interfaces. *AIChE J*. 2005; 51(10):2786–2800.
17. Wylock CE, Cartage T, Colinet P, Haut B. Coupling between mass transfer and chemical reactions during the absorption of CO_2 in a $NaHCO_3$-Na_2CO_3 brine: experimental and theoretical study. *Int J Chem React Eng*. 2008;6:1–22.
18. Wylock CE, Larcy A, Colinet P, Cartage T, Haut B. Direct numerical simulation of bubble-liquid mass transfer coupled with chemical reactions: influence of bubble shape and interface contamination. *Colloids Surf A*. 2011;381(1–3):130–138.
19. Bothe D, Kröger M, Warnecke HJ. A VOF-based conservative method for the simulation of reactive mass transfer from rising bubbles. *Fluid Dyn Mater Process*. 2011;7(3):303–316.
20. Pigeonneau F. Mass transfer of rising bubble in molten glass with instantaneous oxidation-reduction reaction. *Chem Eng Sci*. 2009;64: 3120–3129.
21. Scholze H. *Glass: Nature, Structures and Properties*. Berlin: Springer-Verlag, 1990.
22. Pigeonneau F, Martin D, Mario O. Shrinkage of oxygen bubble rising in a molten glass. *Chem Eng Sci*. 2010;65:3158–3168.
23. Jucha RB, Powers D, McNeill T, Subramanian RS, Cole R. Bubble rise in glassmelts. *J Am Ceram Soc*. 1982;65:289–292.
24. Hornyak EJ, Weinberg MC. Velocity of a freely rising gas bubble in a soda-lime silicate glass melt. *J Am Ceram Soc*. 1984;67:C244–C246.
25. Li KWK, Schneider A. Rise velocities of large bubbles in viscous Newtonian liquids. *J Am Ceram Soc*. 1993;76:241–244.
26. Clift R, Grace JR, Weber ME. Bubbles, Drops, and Particles. New York: Academic Press, 1978.
27. Hadamard J. Mouvement permanent lent d'une sphère liquide et visqueuse dans un liquide visqueux. *C R Acad Sci Paris*. 1911;152: 1735–1738.
28. Rybczynski W. Uber die fortschreitende bewegun einer flussingen kugel in einem zaben medium. *Bull de l'Acad des Sci de Cracovie*. 1911;1:40–46.
29. Levich VG. *Physicochemical Hydrodynamics*. Englewood Cliffs, NJ: Prentice Hall, 1962.
30. Dyke MV. Perturbations Methods in Fluid Mechanics. Stanford, CA: The Parabolic Press, 1975.
31. Ruckenstein E. Mass transfer between a single drop and a continuous phase. *Int J Heat Mass Transfer*. 1967;10:1785–1792.
32. Zeytounian RK. *Modélisation asymptotique en mécanique des fluides newtoniens*. Paris: Springer-Verlag, 1994.
33. Crank J. The Mathematics of Diffusion. Oxford: Clarendon Press, 1956.
34. Pigeonneau F, Muller S. The impact of iron content in oxidation front in soda-lime silicate glasses: an experimental and comparative study. *J Non-Cryst Solids*. 2013;380:86–94.
35. Ern A, Guermond JL. *Eléments finis: Théorie, applications, mise en œuvre*. Paris: Springer, 2002.
36. Hughes TJR, Franca LP, Hulbert GM. A new finite element formulation for computational fluid dynamics: VIII. The Galerkin/least-squares method for advective-diffusive equations. *Comput Methods Appl Mech Eng*. 1989;73:173–189.

37. Hauke G, Hughes TJR. A comparative study of different sets of variables for solving compressible and incompressible flows. *Comput Methods Appl Mech Eng*. 1998;153:1–44.
38. Stoer J, Bulirsch R. Introduction to Numerical Analysis. New York: Springer-Verlag, 1993.
39. Guo W, Labrosse G, Narayanan R. *The Application of the Chebyshev-Spectral Method in Transport Phenomena, Vol. 68 of Lecture Note in Applied and Computational Mechanics*. Berlin: Springer-Verlag, 2012.
40. Collatz L. *The Numerical Treatment of Differential Equations*. Berlin: Springer-Verlag, 1960.

Appendix A: Numerical Methods

Direct numerical solution

Equations (10) and (11), describing the transport phenomena under dimensionless formulation, are solved with a finite element technique. First, the problem must be computed in a finite domain whose geometry is given in Figure A1. The bubble contour Γ_b is centered at the origin of the coordinate system. The position of the outer boundary is adapted to the strength of the convective terms to reduce domain size effect on the solution. When the Péclet number is small, Eqs. (10) and (11) present an elliptic character. In such situation, it is better to take a domain centered on the bubble as illustrated on the left of Figure A1. Conversely, when the Péclet number is larger than 1, the convective terms dominate. In consequence, the outer boundary, $\Gamma_D \cup \Gamma_N$ is not centered on the bubble in order to capture the wake formation near the bubble[20] as it is shown on the right of Figure A1. For the numerical simulations, the radius of the outer boundary is 20 times larger than the bubble radius.

On the bubble surface, the boundary condition is fixed by the physics while the outer domain is divided in two equal sections Γ_D and Γ_N. Furthermore, the boundary conditions on the outer frontier have been adapted to the finite size domain. Indeed, a problem dominated by advection in a finite domain is not well posed if Dirichlet conditions are imposed everywhere.[35] On the contour Γ_D, a Dirichlet condition is imposed both for C_A and C_B, whereas on Γ_N, the cancelation of the diffusive fluxes of C_A and C_B is used. To summarize, the boundary conditions are the following

$$C_A = 1, \frac{\partial C_B}{\partial n} = 0, \quad \text{on } \Gamma_b \tag{A1}$$

$$C_A = C_B = 0, \quad \text{on } \Gamma_D \tag{A2}$$

$$\frac{\partial C_A}{\partial n} = \frac{\partial C_B}{\partial n} = 0, \quad \text{on } \Gamma_N \tag{A3}$$

The finite element method needs a weak formulation of the system of Eqs. (10) and (11). A Galerkin formulation is used which leads to unstable solution when the advection term is dominant. This is due to the lost of elliptic character of the equations. To stabilize the numerical method, the weak formulation is written using a Galerkin/least square method[35,36] which is recommended even to solve partial differential equations yielding shocks.[37]

The computational domain is discretized using triangular elements with a linear interpolation, $\mathbb{P}_1$. When the Péclet and Damköhler numbers become large, a thin boundary layer appears close to the bubble surface, Γ_b. To have high resolution accuracy of the boundary layer, a fine grid is used close to the bubble surface. The minimum size used for this current work is 4×10^{-4} which is enough as the largest values of Péclet and Damköhler numbers are fixed to 10^6 corresponding to a thickness of the boundary layer approximately equal to 10^{-3} (see justification below). Figure A2 presents the mesh around the bubble. With $\mathbb{P}_1$ interpolation, the number of degrees of freedom is equal to 682,650 to solve both equations.

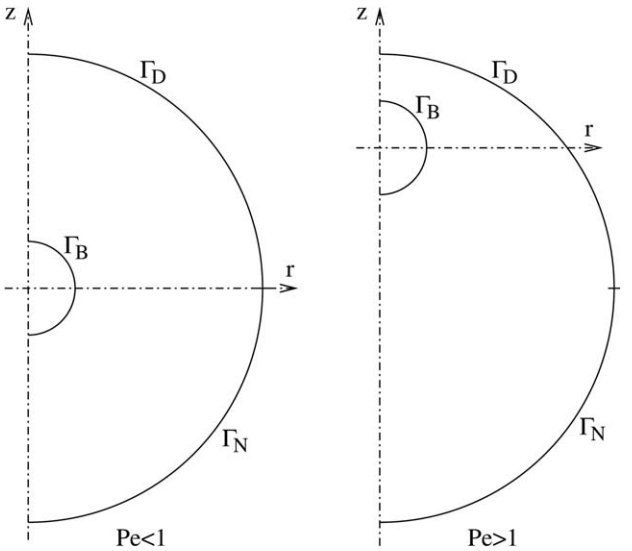

Figure A1. Axisymetric computation domain around a bubble.

The domain on the left is chosen for computations corresponding to Péclet number lower than 1. When the Péclet number is larger than 1, the domain on the right is used to accommodate advection mechanism. The real scale is not respected in this figure. The radius of the outer boundary is 20 times larger than the bubble radius.

Based on the weak formulation, ordinary differential equations form a linear implicit system depending on time solved using backward differentiation formula. This method of second-order accuracy is used with an adaptive time step.[38]

In the following, the problem is solved for Péclet number ranging from 10^{-3} to 10^6, the Damköhler number varies between 1 and 10^6. Three values of the equilibrium constant will be investigated: 10^{-1}, 1, and 10 and two values of the reduced diffusion coefficient of C_B equal to 1/2 and 2.

A coupled finite difference-Chebyshev spectral method to solve the boundary layer equations

A numerical tool of high accuracy level has been developed to solve the boundary layer equations, (26) and (27) with the boundary conditions (28) and (29). Remark that there is no boundary condition on μ which appears only at the first order. Moreover, when $\mu = \pm 1$, that is, at each poles of the bubble interface, the terms proportional to the first derivative in μ disappear. The system of equations is parabolic and can be seen as a Cauchy problem for the μ coordinate. Consequently, the values of C_A and C_B for $\mu = -1$ are used as initial conditions.

We develop a specific numerical method to solve (26) and (27) for which the discretization on ζ is achieved with a Chebyshev-spectral method[39] and a finite difference method on μ with second-order accuracy. For the Chebyshev-spectral method, a collocation method is used for which collocation points are taken following the Gauss-Lobatto distribution.[39] Moreover, the domain has to be truncated on the ζ axis. In numerical simulations, the finite extent is taken between 10 and 100. In the polar direction, a uniform discretization is used. The first derivative in μ is determined following an upward off-centered scheme with three points.[40] The numerical procedure is

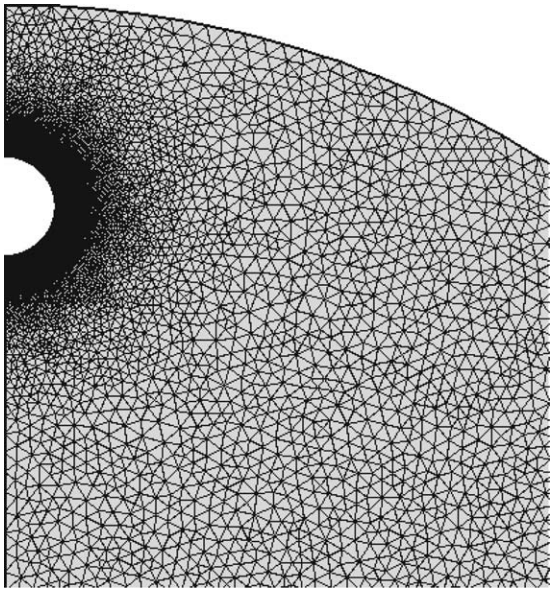

Figure A2. Mesh grid around the bubble (the finest size element is 4×10^{-4} close to the bubble surface when the Péclet number is larger than 1).

based on a fully implicit scheme coupling the two equations on C_A and C_B.

When the chemical reaction is not accounted for, results of this numerical method can be compared to the self-similar solution provided by Levich[29] in order to validate the numerical accuracy of the method. For instance, with a number of collocation points for the spectral method equal to 513 and a resolution on the polar angle of 0.1°, the Sherwood number obtained from the boundary layer numerical solution gives a prefactor equal to 0.65147 to be compared to $2/\sqrt{3\pi}$ of the Levich's solution[29] (see Eq. 32). The relative error is then equal to $4.22\times10^{-6}\%$.

Appendix B: Exact Solutions for Instantaneous Chemical Reaction

Boundary layer regime

To predict the enhancement factor when the chemical reaction kinetics is very fast, the method proposed by Olander[9] can be extended to the boundary layer formulation. When α is larger than 1, chemical equilibrium can be assumed outside the boundary layer for ζ larger than ζ_{eq}. Using a linear combination of Eqs. (26) and (27), the chemical sink and source terms cancel by studying the transport of $C_A+K_{eq}C_B$. Moreover, assuming chemical equilibrium, that is, $C_A=C_B$, we obtain the following equation

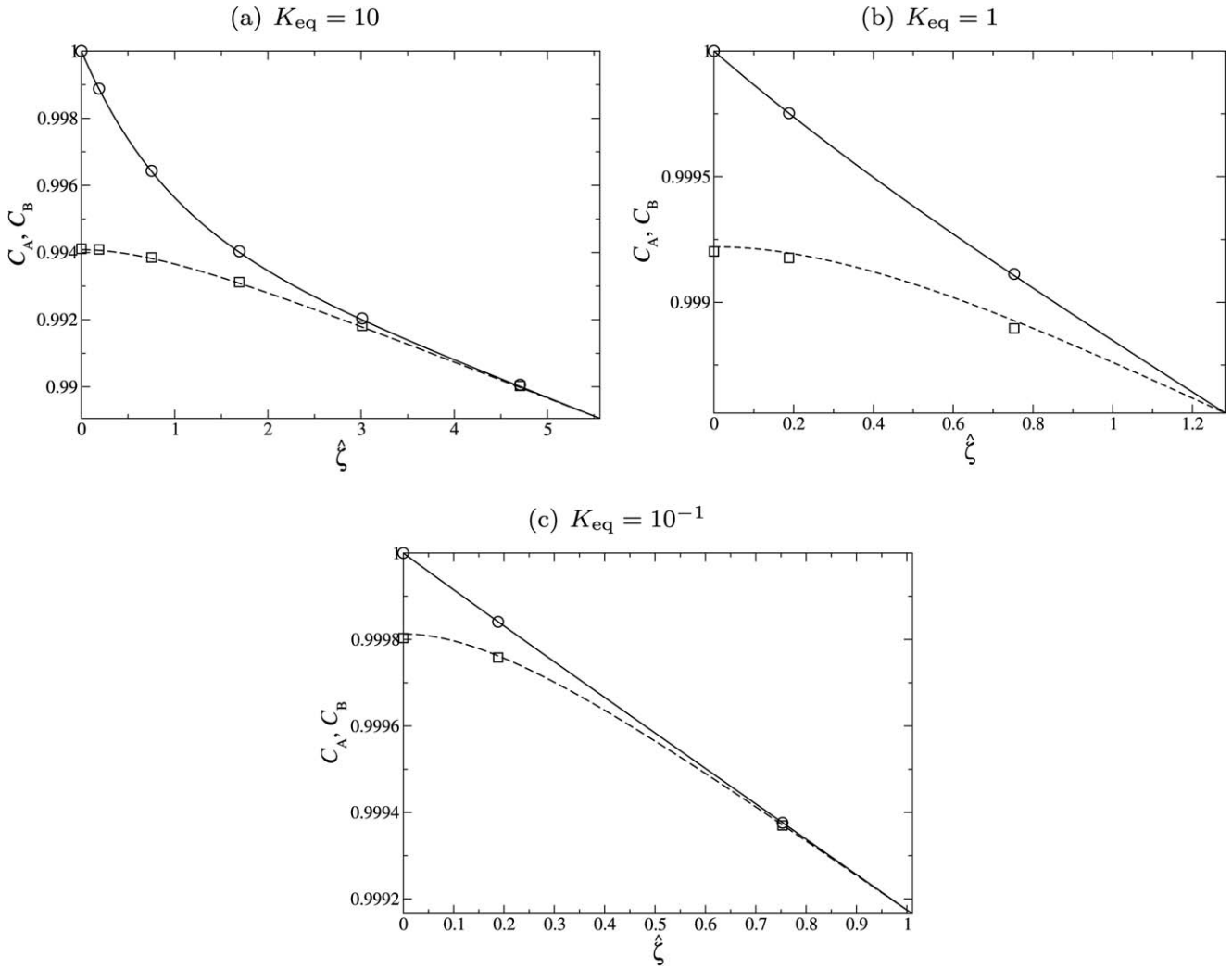

Figure B1. Concentrations obtained from the numerical solution of the boundary layer equations for C_A (○), and C_B (□) vs. $\hat{\zeta}$ when $\alpha = 10^6$ and $\mathcal{D}=1/2$.

The solid line is the asymptotic solution of C_A given by (B9) and the dashed line is the asymptotic solution of C_B given by (B10).

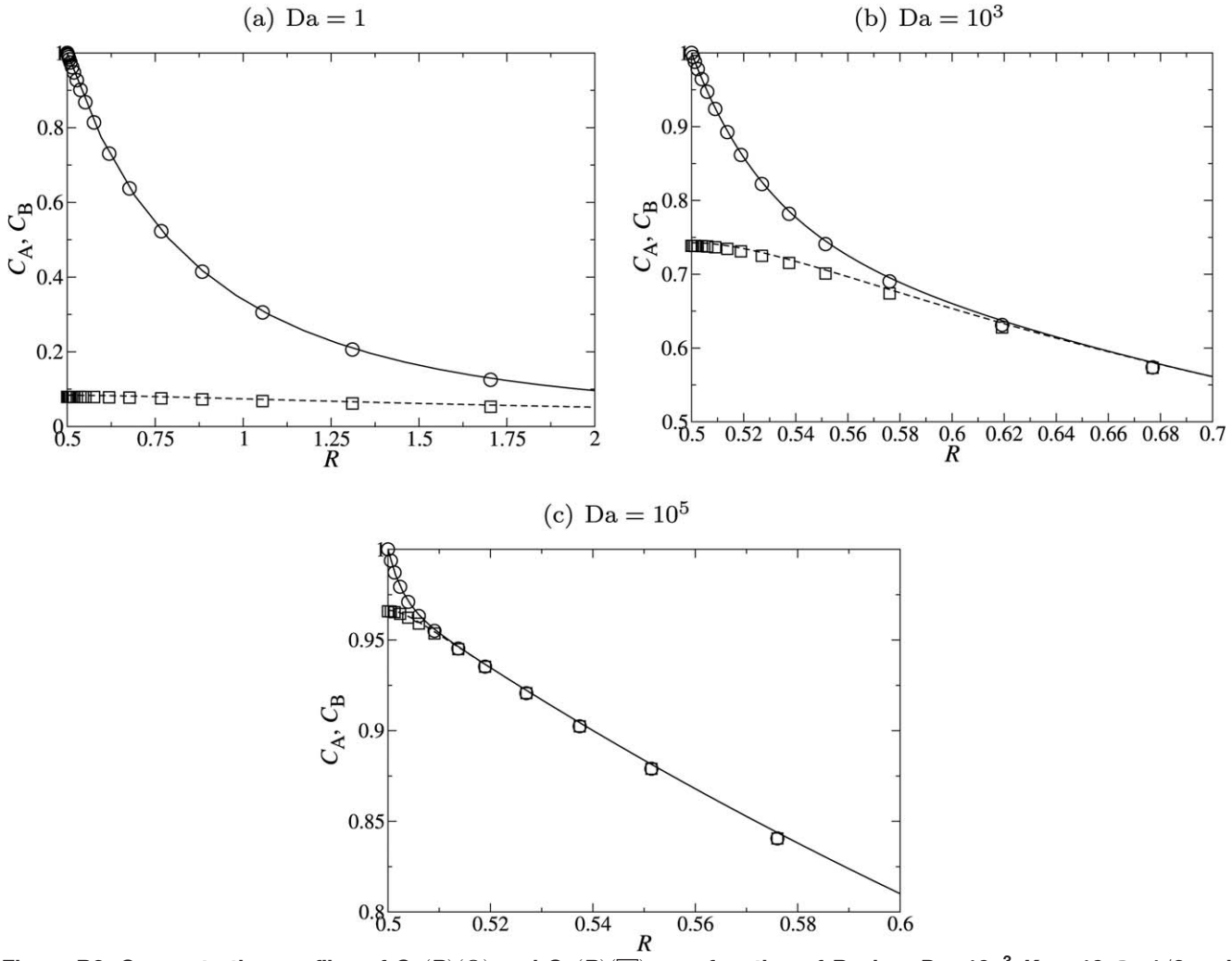

Figure B2. Concentration profiles of $C_A(R)(\bigcirc)$ and $C_B(R)(\square)$ as a function of R when $Pe=10^{-3}, K_{eq}=10, \mathcal{D}=1/2$ and for (a) $Da=1$, (b) $Da=10^3$, and (c) $Da=10^5$.

The solid line is the exact solution for C_A given by Eq. (B5) and the dashed line, the exact solution for C_B given by Eq. (B6).

$$\zeta\mu\frac{\partial C_A}{\partial\zeta}+\frac{1-\mu^2}{2}\frac{\partial C_A}{\partial\mu}=\frac{1+K_{eq}\mathcal{D}}{1+K_{eq}}\frac{\partial^2 C_A}{\partial\zeta^2} \tag{B1}$$

similar to the situation without chemical reaction for which the solution is well known[29] and given by the self-similar relation

$$C_A=\mathrm{erfc}\,(\bar{\eta}) \tag{B2}$$

where the self-similar variable is given by

$$\bar{\eta}=\frac{\zeta}{g(\mu)}\sqrt{\frac{1+K_{eq}}{1+K_{eq}\mathcal{D}}} \tag{B3}$$

The function $g(\mu)$ is given by[29]

$$g(\mu)=2\sqrt{\frac{2}{3}}\frac{\sqrt{2+3\mu-\mu^3}}{1-\mu^2} \tag{B4}$$

The solution (B2) is also valid for C_B. Nevertheless, this solution is not fulfilled in the entire domain as the boundary condition at the bubble interface is not verified for C_B following Eq. (42). So, this solution is only valid outside of ζ_{eq} corresponding to the outer solution. According to the approach of Olander,[9] the outer solution can be used to compute the total mass flux of $C_A+K_{eq}C_B$ given by

$$Sh_{A+K_{eq}B}=\frac{2}{\sqrt{3\pi}}\sqrt{(1+K_{eq})(1+K_{eq}\mathcal{D})}\sqrt{Pe_A} \tag{B5}$$

To establish the inner solution, the inner variable due to the chemical reaction is introduced according to the classical way of the perturbation technique[30]

$$\hat{\zeta}=\zeta\sqrt{\alpha} \tag{B6}$$

In this case, the inner equations become

$$\frac{\partial^2 C_A}{\partial\hat{\zeta}^2}-(C_A-C_B)=0 \tag{B7}$$

$$\mathcal{D}\frac{\partial^2 C_B}{\partial\hat{\zeta}^2}+\frac{1}{K_{eq}}(C_A-C_B)=0 \tag{B8}$$

which are solved exactly with the boundary conditions at the bubble interface and matched to the outer solution for a distance equal to $\hat{\zeta}_{eq}$. The molar concentrations, C_A and C_B, are then given by

$$C_A = A_0 e^{\gamma\hat{\zeta}} + A_1 e^{-\gamma\hat{\zeta}} + A_2\hat{\zeta} + A_3 \tag{B9}$$

$$C_B = A_0 + A_1\hat{\zeta} + A_2(1-\gamma^2)e^{-\gamma\hat{\zeta}} + A_3(1-\gamma^2)e^{\gamma\hat{\zeta}} \tag{B10}$$

where

$$\gamma = \sqrt{\frac{1+K_{eq}\mathcal{D}}{K_{eq}\mathcal{D}}} \tag{B11}$$

and

$$A_1 = -e^{2\gamma\hat{\zeta}_{eq}}A_0, A_2 = -\gamma(1-\gamma^2)\left(1+e^{2\gamma\hat{\zeta}_{eq}}\right)A_0,$$
$$A_3 = 1-\left(1-e^{2\gamma\hat{\zeta}_{eq}}\right)A_0 \tag{B12}$$

$$A_0 = \frac{2\hat{\zeta}_{eq}}{g(\mu)\left[1-e^{2\gamma\hat{\zeta}_{eq}}+(1-\gamma^2)\gamma\left(1+e^{2\gamma\hat{\zeta}_{eq}}\right)\right]}\sqrt{\frac{1+K_{eq}}{\pi\alpha(1+K_{eq}\mathcal{D})}} \tag{B13}$$

Finally, in the inner region the gradient of $C_A + K_{eq}\mathcal{D}C_B$ is constant and equal to A_2 which permits to determine $\hat{\zeta}_{eq}$ by matching the outer solution

$$1-e^{2\gamma\hat{\zeta}_{eq}} + (1-\gamma^2)\gamma\left(1+e^{2\gamma\hat{\zeta}_{eq}}\right)(1-\hat{\zeta}_{eq}) = 0 \tag{B14}$$

This theoretical solution can be used to evaluate the accuracy of the numerical solution of the boundary layer equations. So, three computations have been carried out for $\alpha = 10^6$ when $\mathcal{D}$ is equal to 1/2 and for the equilibrium constant equal to 10, 1, and 10^{-1}. Figure B1 shows the concentration profiles of A and B at the north pole of the bubble, $\mu = -1$, over the range of $\hat{\zeta}_{eq}$ obtained from the numerical solution of the boundary layer formulation (513 collocation points for the spectral method have been used for spatial resolution over ζ coordinate). Solid lines in Figure B1 represent the exact solution given earlier. The numerical solution reproduces very well the asymptotic solution although the thickness of the inner region is very small (10^{-3} when $\alpha = 10^6$). Remark that when the equilibrium constant decreases the thickness over which the inner solution is valid becomes smaller and smaller. The difference between C_B and C_A becomes very small as seen in the scale of y axis in Figure B1. Consequently, the gradient of the C_A at the bubble surface decreases when the equilibrium constant decreases.

Exact Solution of the Transport Equations in a Quiescent Fluid

When advective terms are canceled in Eqs. (17) and (18), the problem is reduced to a coupling between diffusion and reaction where the exact solution can be easily established. The concentration profiles of A and B become independent of θ and take the following forms

$$C_A = \frac{A + Be^{-\beta R}}{R} \tag{B15}$$

$$C_B = \frac{ADa + B(Da-\beta^2)e^{-\beta R}}{Da\,R} \tag{B16}$$

where A and B are determined from the boundary conditions

$$A = \frac{(2+\beta)(Da-\beta^2)}{2\beta[Da-\beta^2-2\beta]}, \quad B = -\frac{Da\,e^{\beta/2}}{\beta[Da-\beta^2-2\beta]} \tag{B17}$$

and β is

$$\beta = \sqrt{\frac{(1+K_{eq}\mathcal{D})Da}{K_{eq}\mathcal{D}}} \tag{B18}$$

Figure B2 presents the concentration profiles $C_A(R)$ and $C_B(R)$ obtained with the finite element method when the Péclet number is equal to 10^{-3}. The equilibrium constant is equal to 10 and $\mathcal{D} = 1/2$. Three values of the Damköhler number are investigated: 1, 10^3, and 10^5. The numerical results obtained for this small value of Péclet number are very well predicted by the exact solution without advection. The mass-transfer enhancement is clearly seen in Figure B2. The region for which the two concentrations are distinct becomes thinner when the Damköhler number increases (remind that $C_A = C_B$ corresponds to chemical reaction at equilibrium). The concentration of C_B at the bubble interface is closer and closer to 1 when Da increases. The slope of C_A rises up strongly as a function of Da.

Manuscript received Dec. 13, 2013, and revision received Mar. 25, 2014.